Nano Res. 2011, 4(4): 360–369
DOI 10.1007/s12274-010-0090-9
Research Article

ISSN 1998-0124
CN 11-5974/O4

Enhanced Photocatalytic Activity of TiO_2 Nanofibers and Their Flexible Composite Films: Decomposition of Organic Dyes and Efficient H_2 Generation from Ethanol–Water Mixtures

Ming-Chung Wu[1, 4], András Sápi[2], Anna Avila[3], Mária Szabó[2], Jussi Hiltunen[3], Mika Huuhtanen[3], Géza Tóth[1], Ákos Kukovecz[2], Zoltán Kónya[2], Riitta Keiski[3], Wei-Fang Su[4], Heli Jantunen[1], and Krisztián Kordás[1] (✉)

[1] Department of Electrical and Information Engineering, University of Oulu, P.O. Box 4500, FI-90014 University of Oulu, Finland
[2] Department of Applied and Environmental Chemistry, University of Szeged, 6720 Szeged, Rerrich Béla tér 1, Hungary
[3] Department of Process and Environmental Engineering, P.O. Box 4300, FI-90014 University of Oulu, Finland
[4] Department of Materials Science and Engineering, National Taiwan University, Taipei 106-17, Taiwan, China

Received: 27 August 2010 / Revised: 1 November 2010 / Accepted: 4 December 2010

ABSTRACT

TiO_2 nanofibers decorated with Pt and Pd nanoparticles have been synthesized and studied in various photocatalytic processes. Excellent photocatalytic behavior in the decomposition of organic dyes in water, degradation of organic stains on the surface of flexible freestanding cellulose/catalyst composite films and in generation of hydrogen from ethanol using both suspended and immobilized catalysts are demonstrated. The performance of the nanofiber-based TiO_2 materials is competitive with—and in some cases outperforms—their conventional nanoparticle-based counterparts. In all cases, Pd-decorated TiO_2 nanoparticles and nanofibers proved to be more efficient than their Pt-based counterparts, which could be explained on the basis of the formation of nano-sized Schottky interfaces at the contacts between TiO_2 and metal nanoparticles. The feasibility of forming cellulose/catalyst composites provides a novel way of utilizing photocatalyst materials in large-area coatings and freestanding films.

KEYWORDS

TiO_2 photocatalyst, metal-decorated TiO_2, nanowires, H_2 generation, oxidation of organic dyes

1. Introduction

Photocatalytic processes can be used to address several aspects of modern renewable energy production and management of environmental pollution. Titanium dioxide (TiO_2) is probably the most promising photocatalyst being environmentally friendly, with low cost, good photocatalytic activity and excellent photostability as demonstrated in electrochemical photolysis of water to produce hydrogen [1–6], in efficient solar cell electrodes [7, 8], in antimicrobial surface coatings [9] and in abatement of volatile organic compounds from air [10]. Decoration of TiO_2 with metals and metal oxides such as Pt [11, 12], Au [11, 13], Pd [14], PdO [14], Ni [15], and Ag [16], and also with carbon nanotubes [17] and graphene [18] has been found to enhance the catalytic and photocatalytic properties and has been exploited in antimicrobial coatings [14], photocatalytic

Address correspondence to lapy@ee.oulu.fi

hydrogen generation from alcohol [11], and in removal of xylene from air [15]. Partial substitution of O in the lattice with N [19–21] or C [22] leads to a shift of the absorption edge towards visible wavelengths thus, enhancing further the photocatalytic efficiency.

Recent results of hydrothermal synthesis of various types of titanate nanofibers and nanotubes synthesized from TiO_2 powders in alkaline solutions [23–29] have opened up new possibilities for large scale and simple production of TiO_2 nanofibers by simply annealing the obtained titanate nanofibers in air. In a number of practical applications, nanofibers can perform much better than the corresponding nanoparticles. In electrical devices employing nanoparticles (e.g., for interconnects, electrodes, field-effect transistor channels, and gas sensing layers) it is vital to have a percolated electrical network of the particles, which is much easier to achieve with elongated 1-dimensional particles than with ordinary 0-dimensional nanoparticles. Furthermore, bundling of nanofibers can also contribute some mechanical robustness to tangled networks and also results in better entanglement with other nanofibers when forming macroscopic films [17, 29, 30].

In this work, anatase nanofibers (TiO_2-NFs) have been synthesized from acid-treated $Na_2Ti_3O_7$ nanofibers by calcination at 600 ˚C and then used as support for Pt and Pd nanoparticles deposited by wet impregnation. Enhanced photocatalytic activity of the metal-decorated TiO_2 nanofibers has been demonstrated by (i) decomposing organic dyes in water, (ii) degrading organic stains on the surface of flexible freestanding composite catalyst films and by (iii) generating hydrogen from ethanol. The results are compared with those obtained using the corresponding catalyst materials based on commercial TiO_2 nanoparticle powders.

2. Experimental

2.1 Catalyst synthesis

Sodium titanate ($Na_2Ti_3O_7$) nanofibers were synthesized through the hydrothermal synthesis route from anatase TiO_2 in aqueous NaOH solution (10 mol/L) at 175 ˚C for 24 h using a rotating autoclave (revolving at 120 r/min around its short axis). Washing of $Na_2Ti_yO_{2y+1}$ in 0.1 mol/L HCl was employed to exchange Na^+-ions in the nanofibers for protons. Finally, the product was washed with deionized water to reach pH ~7 and then filtered and dried in air at 70 ˚C. In order to obtain TiO_2-NFs the product was calcined at 600 ˚C (with a heating rate of 1 ˚C/min) for 12 h. X-ray photoelectron spectroscopy (XPS, Kratos Axis Ultra DLD, mono Al *Kα* source) analysis showed that the exchange of Na^+ by H^+ was only partial, with ~7.3 at% of sodium in the calcined product. Anchoring of Pt and Pd nanoparticles on TiO_2-NFs was carried out by wet impregnation. In a typical process, 20.4 mg of platinum(II) acetylacetonate (Aldrich, 99.99%) or 29.2 mg of palladium(II) acetylacetonate Aldrich, 99%) was dissolved in 200 mL of acetone and mixed with 1.0 g of TiO_2-NFs by ultrasonic agitation for 3 h and then stirring for 6 h. After evaporating the solvent at ~80 ˚C under N_2 atmosphere, the samples were calcined in air at 300 ˚C for 2 h, and then reduced in 15% H_2 (in Ar buffer) flow at 500 ˚C for 4 h to obtain the product, i.e., Pt–TiO_2-NFs and Pd–TiO_2-NFs with ~1 wt% metal loading. Metal-decorated reference samples with a commercial TiO_2 support (referred as Pt–TiO_2 and Pd–TiO_2) were prepared (see Fig. S-1 in the Electronic Supplementary Material (ESM)) using the same routine as employed for the nanofibers.

2.2 Catalyst film fabrication and photocatalytic decomposition of organic stains on the films

Different types of freestanding flexible catalyst films were made by dispersing 70.0 mg of cellulose fibers (Sigma–Aldrich, C6288) and 60.0 mg of each TiO_2-based material (all together 6 different samples) in 20 mL of deionized water by ultrasonic agitation for 30 min followed by stirring for 30 min. The dispersion was then filtered through polycarbonate membranes of 0.2 μm pore size, dried at room temperature for 12 h, and finally detached from the filter.

To mimic decomposition of organic stains on the freestanding flexible catalyst membrane, a highlighting pen (Stabilo Flash, Art. No. 555/24) was used to deposit an organic dye. Each sample was exposed to ultraviolet (UV) light (Philips, HPR 125 W) for 48 h and the fading of the written pattern was recorded with a digital camera.

2.3 Photocatalytic degradation of methyl orange

The photocatalytic activity of TiO_2-NFs, Pt–TiO_2-NFs,

Pd–TiO_2-NFs, and the reference TiO_2, Pt–TiO_2, Pd–TiO_2 photocatalyst materials (based on commercial Degussa P25 TiO_2) were tested in the decoloration of methyl orange, widely used as a model reaction in photocatalysis. In a typical experiment, 10.0 mg of catalyst was sonicated for 2 min in 10 mL of methyl orange (Reanal) aqueous solution having a concentration of 10 mg/L. The suspension was irradiated with UV light (mercury-vapor lamp, 80 W) under vigorous stirring under ambient conditions. After centrifugation (for 15 min at 3200 r/min) the UV–Vis spectrum of the remaining methyl orange in the supernatant was recorded (Hitachi U-2001, UV–Vis spectrophotometer) in the 200–700 nm wavelength range. The methyl orange concentration was calculated from the absorbance at λ = 464 nm, employing a previously plotted calibration curve.

2.4 Hydrogen generation from ethanol–water mixtures

Photocatalytic hydrogen generation tests were carried out using a 1:3 molar ratio mixture of ethanol and water (1 L) in which 0.2 g of TiO_2-based catalyst was suspended before each experiment. The temperature of the mixture was kept near room temperature (23 °C ± 1 °C) using a thermostat. As the light source, 6 UVB lamps (Sankyo Denki, G15T8E, I_{max} at λ ~313 nm, P_{UV}~3 W) were placed in a hexagonal arrangement around the reactor. In order to avoid sedimentation of the catalyst powder, the reaction liquid was circulated by pumping. In addition, N_2 gas was bubbled through the reactor with a flow rate of 400 mL/min, serving also as a purging gas for the evolved gaseous products. The outlet of the reactor was connected to cold traps and to a molecular sieve (to condense and remove the vapours of water and ethanol), and then to a hydrogen analyser (General Electric, XMTC-6C-11). The illumination time was 60 min in each experiment. In addition, hydrogen production rates over Pt and Pd decorated TiO_2-NF catalysts were measured with different irradiation powers by switching on 2, 4 or 6 lamps (each lamp was located at the corner of a hexagon around the reactor) during the measurement. In this test, 15 min irradiation times were applied.

Experiments using immobilized catalyst were also implemented. Each catalyst powder (25 mg) was mixed with 25 mg cellulose, then suspended in water and finally deposited on the surface of a filter paper (~12 cm in diameter) by drop casting. The dried catalyst-coated paper sheets were then folded into cylinders and fixed in the tube reactor. Similar experiments to those described above were performed (Fig. S-2 in the ESM).

2.5 Structural characterization of the materials

The microstructure of composite films and diameter/structure of individual nanofibers and the decorating metal nanoparticles were studied by field-emission scanning electron microscopy (FESEM, Jeol JSM-6300F), by transmission electron microscopy combined with electron diffraction (EFTEM, LEO 912 Omega, 120 kV) as well as by X-ray diffraction (XRD, Siemens D5000 and Philips PW 1380, both using Cu $K\alpha$ radiation).

3. Results and discussion

In order to prepare the catalytically active anatase TiO_2 nanofibers from the sodium hydrogen titanate nanofibers, a quick screening was carried out to find the appropriate calcination temperature. The samples were heated in air at 400, 550, 600, 750, and 850 °C for 2 h then analyzed by X-ray diffraction as shown in Fig. 1(a). Calcination at temperatures up to 600 °C resulted in the formation of an anatase phase only. The intensity of reflections increased with temperature, indicating better ordering of the lattice. However at temperatures above 600 °C, formation of the catalytically inactive rutile phase starts, as shown by the appearance of its (110) reflection at ~27.2° 2θ [PDF #77-0445]. To optimize the calcination conditions further—i.e., to improve the crystallinity of the anatase phase without forming rutile—we calcined samples at 600 °C for 12 h using two different heating rates (1 and 5 °C/min). The appearance of reflections from low intensity higher index planes in the diffraction patterns clearly demonstrates the beneficial effect of prolonged calcination on the formation of highly crystalline anatase (Fig. 1(b)). All the peaks can be perfectly indexed as the body-centered tetragonal lattice structure [JCPDS No. 89-4921] of TiO_2, with lattice constants $a = b = 3.78$ Å and $c = 9.50$ Å. Although the heating rate seems to have only minor effect on crystallinity (slightly better crystal formation when the

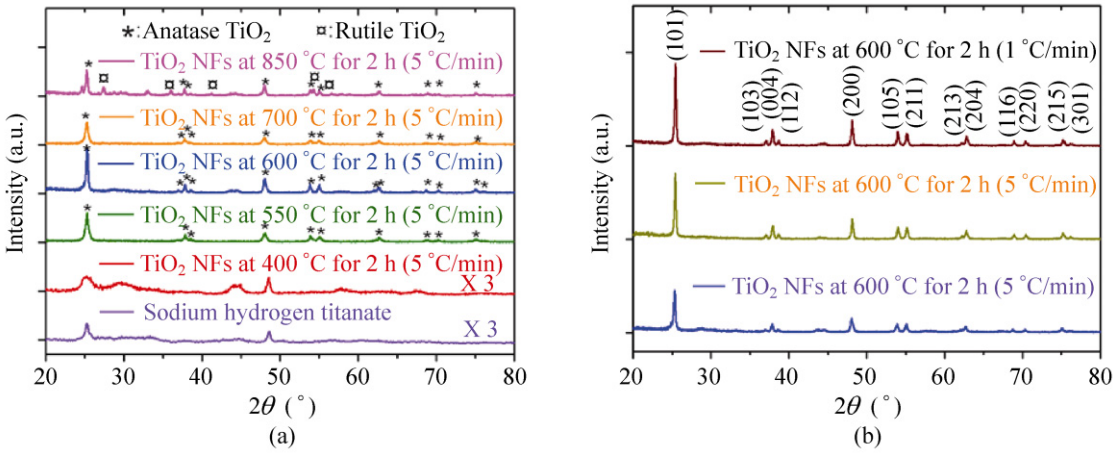

Figure 1 (a) X-ray diffraction patterns of sodium hydrogen titanate nanofibers calcined in air at 400, 550, 600, 750, and 850 °C for 2 h (heating rate of 5 °C/min). (b) Sodium hydrogen titanate nanofibers calcined for 2 h (heating rate of 5 °C/min) and for 12 h (heating rates of 1 and 5 °C/min)

lower heating rate was employed), we decided to use the lower heating throughout this work to synthesize the TiO_2 nanofibers serving as starting materials for our photocatalysts.

The as-made pristine anatase nanofibers had a length of up to a few micrometers and a diameter of ~50 nm (Fig. 2). Decoration of anatase TiO_2 nanofibers was obtained by wet impregnation with metal acetylacetonates followed by decomposition in air at 300 °C and reduction in hydrogen at 500 °C. The weak and broadened XRD reflections found at 2θ ~40° for both Pt and Pd-based catalysts can be assigned to metallic Pd(111) and Pt(111), and suggest very small size nanoparticles are present (Fig. S-3 in the ESM). Based on TEM analysis, the Pt and Pd nanoparticles are homogeneously distributed on the surface of TiO_2 nanofibers and show uniform size distributions with average particle diameters of 2.3 nm ± 0.5 nm and 3.8 nm ± 1.1 nm, respectively.

The photocatalytic activities of the synthesized TiO_2-based materials (pristine TiO_2-NFs, TiO_2 powder, and their Pd- and Pt-decorated derivatives) were tested by UV light-induced photodegradation of methyl orange in aqueous solution. UV–Vis spectra of methyl orange as function of UV light irradiation time were recorded (Fig. 3), and from the absorbance measured at $\lambda = 464$ nm the corresponding dye concentration could be calculated using a calibration curve measured previously. TiO_2-catalyzed photodegradation of different dyes essentially follows Langmuir–Hinshelwood kinetics, which can be simplified to an apparent first-order kinetics at lower initial dye concentrations,

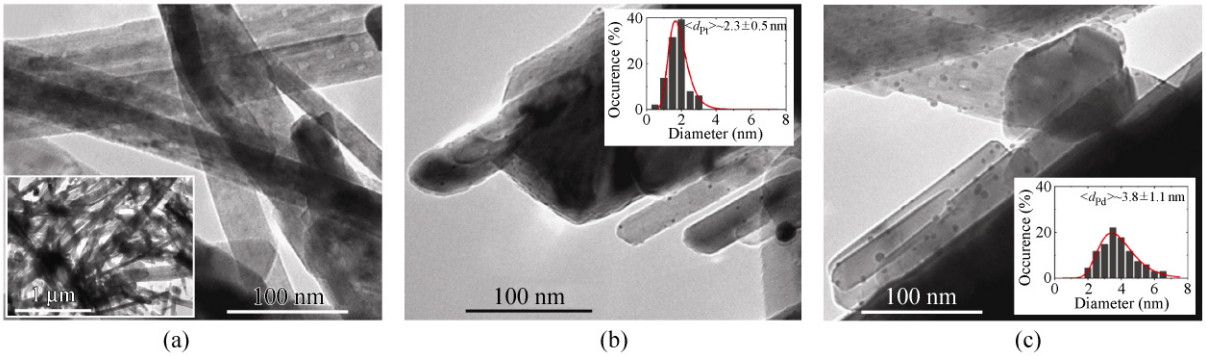

Figure 2 TEM images of (a) pristine, (b) 1.0 wt% Pt-decorated, and (c) 1.0 wt% Pd-decorated TiO_2 nanofibers. Insets in panels (b) and (c) show the corresponding Pt and Pd metal nanoparticle size distributions

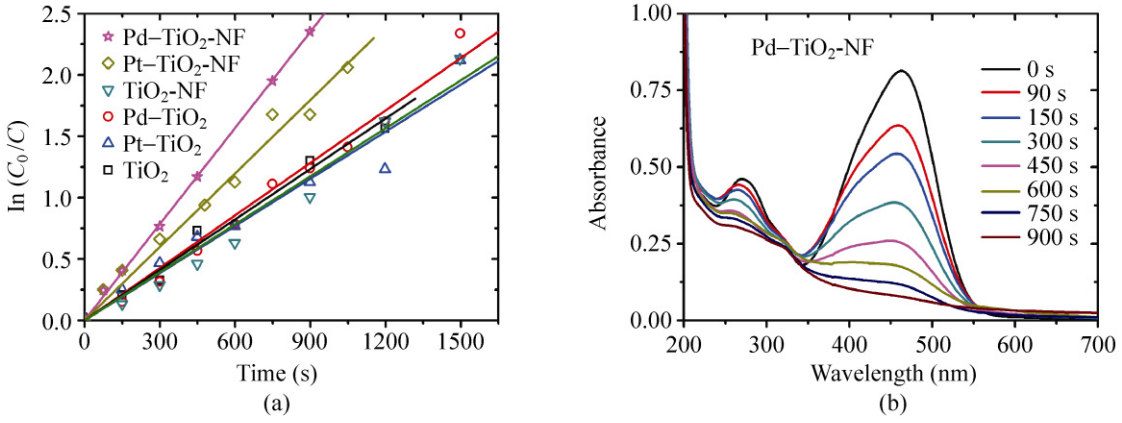

Figure 3 (a) Linearized kinetic plots for the degradation of methyl orange using different types of TiO_2-based catalyst materials. (b) UV–Vis absorbance spectra of methyl orange (initial concentration of 10.0 mg/L) as a function of illumination time with the Pd–TiO_2-NF catalyst (10.0 mg dispersed in 10 mL of solution)

mathematically described as $\ln(c_0 / c) = kt$, where c is the concentration of the dye at time t, c_0 is the initial concentration and k is the apparent reaction rate constant [31]. Plotting the logarithm of the reciprocal of the measured dye concentration as a function of time, we obtain linear slopes for each catalyst we studied, in good agreement with the Langmuir–Hinshelwood model. Pristine TiO_2 nanofibers show almost the same activity as commercial TiO_2 and its Pt- and Pd-sensitized derivatives. Despite the fact that the enhancement in the rate of methyl orange photodegradation was negligible when noble metals were decorated on TiO_2 nanoparticles (the reaction rate constants were all ~0.08 min^{-1} for the pristine TiO_2 and metal-decorated species), the effects on the photocatalytic activity of metal addition to TiO_2 nanofibers were found to be considerable. The apparent rate constants with Pt–TiO_2-NFs and Pd–TiO_2-NFs were measured to be ~0.12 min^{-1} and ~0.16 min^{-1}, respectively.

Table 1 Reaction rate constants for the photodegradation of methyl orange over different TiO_2-based catalysts

Sample	k (min^{-1})
Pd–TiO_2-NFs	0.156 ± 0.001
Pt–TiO_2-NFs	0.120 ± 0.003
TiO_2-NFs	0.078 ± 0.003
Pd–TiO_2	0.085 ± 0.002
Pt–TiO_2	0.077 ± 0.004
TiO_2	0.082 ± 0.003

In earlier work, metals such as Au, Pt, and Pd attached on TiO_2 nanoparticles have been shown to help in achieving better activity of the catalyst due to the rectifying Schottky barrier formed at the interface between metal nanoparticles and TiO_2 [32–34]. Considering the electron affinity of TiO_2 (χ = 3.9 eV) and the work functions of Pt (ϕ_{Pt} = 5.7 eV) and Pd (ϕ_{Pd} = 5.1 eV) the barrier heights are 1.8 eV and 1.2 eV, respectively. Photogeneration of electrons and holes takes place by the absorption of high energy photons followed by charge separation. Since the electrons at the higher energy levels in the conduction band of TiO_2 can pass through the interface (while electron injection from metal to semiconductor is limited by the Schottky barrier), a much more efficient separation of charges with lower recombination rates is expected than that in pristine TiO_2 [35]. As a result, the negatively charged metal nanoparticles contribute to chemical reduction of protons adsorbed on their surfaces; meanwhile in the proximity of the metal nanoparticles, the depleted (i.e., positively charged) TiO_2 surface enhances oxidative processes (see Scheme 1 for an illustration using the generation of hydrogen by oxidation of ethanol as an example). The lower Schottky barrier at the contact of TiO_2 and Pd (as compared to that with Pt) may explain the better photocatalytic activity of the Pd-based catalysts in our experiments.

Using photocatalysts to degrade organic compounds on surfaces has attracted considerable attention in the

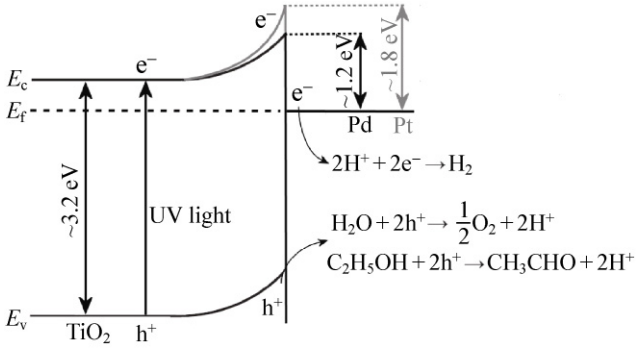

Scheme 1 Mechanism of photocatalytic generation of hydrogen from ethanol aqueous solution over Pt/TiO_2 and Pd/TiO_2 catalysts as a consequence of optical electron–hole pair generation, and efficient charge separation induced by the Schottky interface between metal nanoparticles with large work function and *n*-type semiconducting TiO_2 [36–38]. Protons formed by the reaction between holes and water, as well as organic compounds, are reduced by electrons injected previously into the metal nanoparticles

recent years, due to possible applications in self-cleaning coatings and antimicrobial surfaces [39–42]. In this study, we used cellulose nanofibers and the TiO_2-based catalysts to prepare composite films that enable easy handling and use of the metal-decorated TiO_2 catalysts. Using the catalyst composite films we demonstrated degradation of organic dyes deposited on the surface of thin catalyst membranes as shown in Fig. 4. A letter "A" was written on each cellulose–catalyst composite film with a highlighting pen, and then the membranes were exposed to UV light (Philips, HPR 125 W) for 48 h. The composite membranes consisting of only cellulose and TiO_2 or TiO_2-NFs showed only minor changes in the intensity of the color pattern, whereas, the other films—in which also Pd and Pt nanoparticles were present—degraded the deposited ink considerably. In the case of the cellulose/Pd–TiO_2-NFs and cellulose/Pt–TiO_2-NFs composites, the original stain could hardly be seen, i.e., fading of the dye was practically complete.

In each composite, the cellulose microfibers were uniformly coated with the catalyst materials as shown in Fig. 5. The composites are flexible and can be folded until reaching a curvature radius of ~5 mm (when the membrane buckles and then breaks). The composites with TiO_2 nanoparticles are significantly softer than

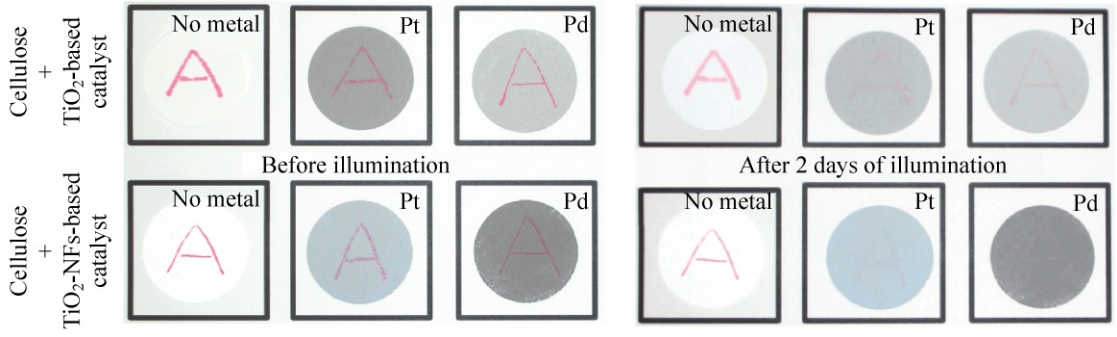

Figure 4 Photographs of TiO_2-based catalyst/cellulose composite films showing the degradation of an organic dye in a colored ink deposited on the surface. Each membrane (diameter of ~38 mm) was obtained by filtration of an aqueous dispersion of 70 mg of cellulose and 60 mg of TiO_2 or TiO_2-NFs-based catalyst (the Pd or Pt content was 0.6 mg)

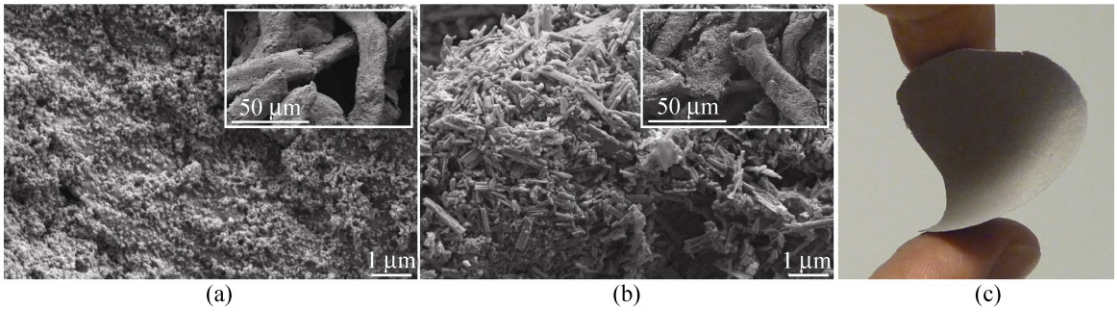

Figure 5 Scanning electron micrographs of cellulose fiber surfaces. (a) Cellulose/Pt–TiO_2 and (b) cellulose/Pt–TiO_2-NFs composites. Insets show lower magnification electron micrographs of the corresponding films. (c) Photograph of a bent composite membrane

those made of the nanofibers. The difference in stiffness is unexpected since the typical dimensions of the cellulose fibers (lengths of hundreds of micrometers and diameters between 10 and 25 μm) are about 3 orders of magnitude larger than those of the TiO_2 nanofibers (lengths of a few micrometers, and diameters between 20 and 60 nm), which rules out a conventional mechanical tangling. However, the presence of TiO_2 with different shapes in the different types of catalyst materials can influence mechanical friction and sticking of adjacent cellulose fibers coated with the nanoparticles, thus, affecting flexibility.

Figure 6(a) shows hydrogen production over 1 wt% Pd- and Pt-decorated TiO_2 and TiO_2-NF catalysts using UV–B irradiation. The rate of hydrogen formation was found to be highest over Pd/TiO_2. Pd- and Pt-decorated TiO_2-NF catalysts showed slightly lower hydrogen production than the corresponding metal-decorated TiO_2 catalysts. Pd was observed to be more active material than Pt. The rate of hydrogen formation was found to be around 1500 μmol/h for Pd/TiO_2, 950 μmol/h for Pd/TiO_2-NF, 750 μmol/h for Pt/TiO_2, and 450 μmol/h for Pt/TiO_2-NF. The rate of hydrogen formation over parent TiO_2 and TiO_2-NF was very low (< 30 μmol/h in each case). These results are in agreement with those previously reported in the Ref. [43, 44].

The differences between the activities of the corresponding nanofiber- and nanoparticle-based catalyst materials may have several origins. The nanoparticle-based catalyst consists of both anatase and rutile phases, unlike the nanofibers used here, which were entirely anatase [45]. Since the two phases show different activities in various photochemical processes, this might be one reason for the measured differences in the decomposition of organic dyes as well as in the generation of H_2. On the other hand, due to the elongated shape of the nanofibers, the surface area of the planes in the apices as a fraction of the overall surface area is much smaller than that for short nanorods or nearly spherical nanoparticles. Different facets of a single crystal exhibit distinctive physical and chemical properties, thus, giving rise to the different activities of anatase nanoparticles of different shapes [46, 47].

The effect of illumination power on H_2 production using Pd- and Pt-loaded TiO_2-NF catalysts is shown in Fig. 6(b). Increasing the illumination power clearly leads to an increase in the formation of hydrogen. The lamps were successively switched on in pairs, i.e., using 2, 4, and then 6 lamps. The curves indicate that a change in illumination power has an immediate effect on the hydrogen formation rate. However, the hydrogen production rates show a nonlinear dependence on intensity, which may be due to optical saturation of the absorber or a consequence of the non-uniform illumination caused by the geometry of the experimental setup.

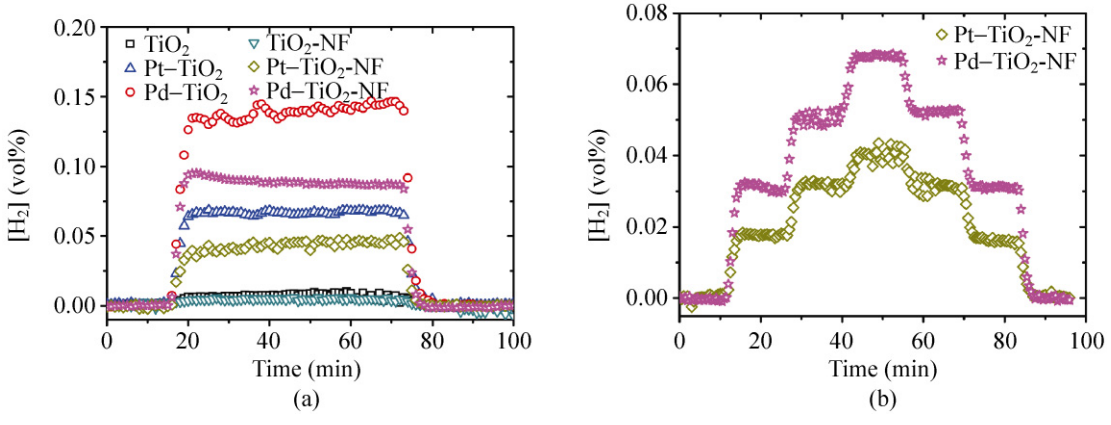

Figure 6 (a) Hydrogen formation over parent and metal-loaded (1 wt%) catalyst materials (0.2 g of each) using an ethanol:water (molar ratio 1:3) mixture with UV–B irradiation (6 lamps). (b) Effect of illumination power on hydrogen formation (using 0, 2, 4, 6, 4, 2, and 0 lamps in succession) for Pd/TiO_2-NF and Pd/TiO_2-NF catalysts

4. Conclusions

TiO_2 nanofibers decorated either with Pt or Pd nanoparticles show excellent photocatalytic behavior, as demonstrated by the decomposition of organic dyes in water, degradation of organic stains on the surface of flexible freestanding cellulose/catalyst composite films and generation of hydrogen from ethanol using both suspended and immobilized catalysts. The performance of the nanofiber-based catalyst materials is competitive with—and in some cases outperforms—their conventional nanoparticle-based counterparts. In all cases, Pd decorated TiO_2 nanoparticles and nanofibers proved to be more efficient than their Pt-based counterparts, making the Pd-based catalysts more industrially relevant especially when we consider the lower cost of Pd metal (approximately 20%–25% of that of Pt metal). Furthermore, the ability to fabricate cellulose/catalyst composites suggests a novel way of utilizing photocatalyst materials in large-area coatings and freestanding films, which could be produced (after some optimization of cellulose/catalyst size and amount) in extremely large quantities, e.g., by roll-to-roll processes employed by the paper and printing industries. Preliminary experiments conducted using immobilized catalyst materials deposited on large area filter papers showed similar catalytic activity in H_2 generation as the powder samples (Fig. S-2 in the ESM).

Acknowledgements

We thank Dr. Andrey Shukarev and Prof. Jyri-Pekka Mikkola for the XPS analysis. The authors are grateful for financial support received from the Finnish Funding Agency for Technology and Innovation (TEKES) (projects No. 52423 and 52433) and Academy of Finland (projects No. 120853, 124357, 128626, and 128908), the Hungarian Scientific Research Fund (OTKA projects No. NNF-78920 and 73676) and the "National Science Council of Taiwan" (projects No. 98-3114-E-002-001 and 99-2120-M-002-011).

Electronic Supplementary Material: Supplementary material (EFTEM images of Pt and Pd nanoparticles supported on TiO_2 nanoparticles, images of cellulose/Pt–TiO_2-NFs composite films and measurement data for hydrogen production as well as X-ray diffraction patterns of TiO_2-NFs, Pt–TiO_2-NFs, and Pd–TiO_2-NFs samples) is available in the online version of this article at http://dx.doi.org/10.1007/s12274-010-0090-9.

References

[1] Fujishima, A.; Honda, K. Electrochemical photolysis of water at a semiconductor electrode. *Nature* **1972**, *238*, 37–38.

[2] Nozik, A. J. Photoelectrolysis of water using semiconducting TiO_2 crystals. *Nature* **1975**, *257*, 383–386.

[3] Zhang, J.; Du, P.; Schneider, J.; Jarosz, P.; Eisenberg, R. Photogeneration of hydrogen from water using an Integrated system based on TiO_2 and platinum(II) diiminde dithiolate sensitizers. *J. Am. Chem. Soc*. **2007**, *129*, 7726–7727.

[4] Hoffmann, M. R.; Martin, S. T.; Choi, W.; Bahnemann, D. W. Environmental applications of semiconductor photocatalysis. *Chem. Rev.* **1995**, *95*, 69–96.

[5] Linsebigler, A. L.; Lu, G. Q.; Yates, J. T. Photocatalysis on TiO_2 surfaces: Principles, mechanisms, and selected results. *Chem. Rev.* **1995**, *95*, 735–758.

[6] Fox, M. A.; Dulay, M. T. Heterogeneous photocatalysis. *Chem. Rev.* **1993**, *93*, 341–357.

[7] Bwana, N. N. Effects of the morphology of the electrode nanostructures on the performance of dye-sensitized solar cells. *Nano Res.* **2008**, *1*, 483–489.

[8] Fan, Z.; Ruebusch, D. J.; Rathore, A. A.; Kapadia, R.; Ergen, O.; Leu, P. W.; Javey, A. Challenges and prospects of nanopillar-based solar cells. *Nano Res.***2009**, *2*, 829–843.

[9] Fu, G. F.; Vary, P. S.; Lin, C. T. Anatase TiO_2 nanocomposites for antimicrobial coatings. *J. Phys. Chem. B* **2005**, *109*, 8889–8898.

[10] Peral, J.; Ollis, D. F. Heterogeneous photocatalytic oxidation of gas-phase organics for air purification: Aceton, 1-butanol, butyraldehyde, formaldehyde, and *m*-xylene oxidation. *J. Catal.* **1992**, *136*, 554–565.

[11] Bamwenda, G. R.; Tsubota, S.; Nalamura, T.; Haruta, M. Photoassisted hydrogen production from water–ethanol solution: A comparison of activities of Au–TiO_2 and Pt–TiO_2. *J. Photochem. Photobiol. A: Chem.* **1995**, *89*, 177–189.

[12] Wu, G.; Chen, T.; Zong, X.; Yan, H.; Ma, G.; Wang, X.; Xu, Q.; Wang, D.; Lei, Z.; Li, C. Suppressing CO formation by anion adsorption and Pt deposition on TiO_2 in H_2 production from photocatalytic reforming of methanol. *J. Catal.* **2008**, *253*, 225–227.

[13] Rosseeler, O.; Shankar, M. V.; Du, M. K. L.; Schmidlin, L.; Keller, N.; Keller, V. Solar light photocatalytic hydrogen production from water over Pt and Au/TiO_2(anatase/rutile)

photocatalysts: Influenceof noble metal and porogen promotion. *J. Catal.* **2010**, *269*, 179–190.

[14] Li, Q.; Li, Y. W.; Wu, P.; Xie, R.; Shang, J. K. Palladium oxide nanoparticles on nitrogen-doped titanium oxide: Accelerated photocatalytic disinfection and post-illumination catalytic "memory". *Adv. Mater.* **2008**, *20*, 3717–3723.

[15] Tseng, H. H.; Wei, M. C.; Hsiung, S. F.; Chiou, C. W. Degradation of xylene vapor over Ni-doped TiO_2 photocatalysts prepared by polyol-mediated synthesis. *Chem. Eng. J.* **2009**, *150*, 160–167.

[16] Hirakawa, T.; Kamat, P. V. Charge separation and catalytic activity of Ag@TiO_2 core–shell composite clusters under UV-irradiation. *J. Am. Chem. Soc.* **2005**, *127*, 3928–3934.

[17] Woan, K.; Pygiotakis, G.; Sigmund, W. Photocatalytic carbon-nanotube-TiO_2 composites. *Adv. Mater.* **2009**, *21*, 2233–2239.

[18] Zhang, H.; Lv, X.; Li, Y.; Wang, Y.; Li, J. P25-graphene composite as a high performance photocatalyst. *ACS Nano* **2010**, *4*, 380–386.

[19] Asahi, R.; Morikawa, T.; Ohwaki, T.; Aoki, K.; Taga, Y. Visible-light photocatalysis in nitrogen-doped titanium oxides. *Science* **2001**, *293*, 269–271.

[20] Burda, C.; Lou, Y.; Chen, X.; Samia, A. C. S.; Stout, J.; Gole, J. L. Enhanced nitrogen doping in TiO_2 nanoparticles. *Nano Lett.* **2003**, *3*, 1049–1051.

[21] Khan, S. U. M.; Al-Shahry, M.; Ingler Jr, W. B. Efficient photochemical water splitting by a chemically modified *n*-TiO_2. *Science* **2002**, *297*, 2243–2245.

[22] Sakthivel, S.; Kisch, H. Daylight photocatalysis by carbon-modified titanium dioxide. *Angew. Chem. Int. Ed.* **2003**, *42*, 4908–4911.

[23] Horvath, E.; Kukovecz, A.; Konya, Z.; Kiricsi, I. Hydrothermal conversion of self-assembled titanate nanotubes into nanowires in a revolving autoclave. *Chem. Mater.* **2007**, *19*, 927.

[24] Zhang, P.; Yin, S.; Petrykin, M.; Kakihana, M.; Sato, T. Preparation of high performance fibrous titania photocatalysts by solvothermal reaction of protonated form of tetratitanate. *J. Mol. Catal. A* **2009**, *309*, 50–56.

[25] Chuangchote, S.; Jitputti, J.; Sagawa, T.; Yoshikawa, S. Photocatalytic activity for hydrogen evolution of electrospun TiO_2 nanofibers. *ACS Appl. Mater. Interfaces* **2009**, *1*, 1140–1143.

[26] Feist, T. P.; Davies, P. K. The soft chemical synthesis of TiO_2(B) from layered titanates. *J. Solid State Chem.* **1992**, *101*, 275–295.

[27] Zhang, S.; Chen, Q.; Peng, L. M. Structure and formation of $H_2Ti_3O_7$ nanotubes in an alkali environment. *Phys. Rev. B* **2005**, *71*, 014104.

[28] Tian, Z. R. R.; Voigt, J. A.; Liu, J.; McKenzie, B.; Xu, H. F. Large oriented arrays and continuous films of TiO_2-based nanotubes. *J. Am. Chem. Soc.* **2003**, *125*, 12384–12385.

[29] Wang, Y. M.; Du, G. J.; Liu, H.; Liu, D.; Qin, S. B.; Wang, N.; Hu, C. G.; Tao, X. T.; Jiao, J.; Wang, J. Y.; Wang, Z. L. Nanostructured sheets of Ti–O nanobelts for gas sensing and antibacterial applications. *Adv. Funct. Mater.* **2008**, *18*, 1131–1137.

[30] Wang, D.; Liu, Y.; Wang, C.; Zhou, F.; Liu, W. Highly flexible coaxial nanohybrides made from porous TiO_2 nanotubes. *ACS Nano* **2009**, *3*, 1249–1257.

[31] Katti, A.; Venna, S. R.; Carreon, M. A. Self-assembly hydrothermal assisted synthesis of mesoporous anatase in the presence of ethylene glycol. *Catal. Comm.* **2009**, *10*, 2036–2040.

[32] Uosaki, K.; Yoneda, R.; Kita, H. Effect of platinization on the electrochemical behavior of titanium dioxide electrode in aqueous solution. *J. Phys. Chem.* **1985**, *89*, 4042–4046.

[33] Chen, X.; Mao, S. S. Titanium dioxide nanomaterials: Synthesis, properties, modification, and application. *Chem. Rev.* **2007**, *107*, 2891–2959.

[34] Yoon, J. W.; Sasaki, T.; Koshizaki, N. Dispersion of nanosized noble metals in TiO_2 matrix and their photoelectrode properties. *Thin Solid Films* **2005**, *483*, 276–282.

[35] Park, J. Y.; Renzas, J. R.; Contreras, A. M.; Somorjai, G. A. The genesis and importance of oxide-metal interface controlled heterogeneous catalysis; the catalytic nanodiode. *Topics in Catalysis* **2007**, *46*, 217–222.

[36] Kuo, H. L.; Kuo, C. Y.; Liu, C. H.; Chao, J. H.; Lin, C. H. A highly active bi-crystalline photocatalyst consisting of TiO_2(B) nanotube and anatase particle for producing H_2 gas from neat ethanol. *Catal. Lett.* **2007**, *113*, 7–12.

[37] Yang, Y. Z.; Chang, C. H.; Idriss, H. Photo-catalytic production of hydrogen form ethanol over M/TiO_2 catalysts (M = Pd, Pt or Rh). *Appl. Catal. B: Environmental* **2006**, *67*, 217–222.

[38] Moon, S. C.; Mametsuka, H.; Tabata, S.; Suzuki, E. Photocatalytic production of hydrogen from water using TiO_2 and B/TiO_2. *Catal. Today.* **2000**, *58*, 125–132.

[39] Macak, J. M.; Zlamal, M.; Krysa, J.; Schmuki, P. Self-organized TiO_2 nanotube layers as highly efficient photocatalysts. *Small* **2007**, *3*, 300–304.

[40] Ohko, Y.; Utsumi, Y.; Niwa, C.; Tatsuma, T.; Kobayakawa, K.; Satoh, Y.; Kubota, Y.; Fujishima, A. Self-sterilizing and self-cleaning of silicone catheters coated with TiO_2 photochatalyst thin films: A preclinical work. *J. Biomed. Mater. Res. B* **2001**, *58*, 97–101.

[41] Miyauchi, M.; Nakajima, A.; Hashimoto, K.; Watanabe, T. A highly hydrophilic thin film under 1 μW/cm^2 UV illumination. *Adv. Mater.* **2000**, *12*, 1923–1927.

[42] Dong, W.; Cogbill, A.; Zhang, T.; Ghosh, S.; Tian, Z. R. Multifunctional, catalytic nanowire membranes and the membrane-based 3D devices. *J. Phys. Chem. B* **2006**, *110*, 16819–16822.

[43] Lin, C. H.; Chao, J. H.; Liu, C. H.; Chang, J. C.; Wang, F. C. Effect of calcination temperature on the structure of a Pt/TiO_2 (B) nanofiber and its photocatalytic activity in generating H_2. *Langmuir* **2008**, *24*, 9907–9915.

[44] Wang, F. C.; Liu, C. H.; Liu, C. W.; Chao, J. H.; Lin, C. H. Effect of Pt loading order on photocatalytic activity of Pt/TiO_2 nanofiber in generation of H_2 from neat ethanol. *J. Phys. Chem. C.* **2009**, *113*, 13832–13840.

[45] Ohnoa, T.; Sarukawaa, K.; Tokiedaa, K.; Matsumura, M. Morphology of a TiO_2 photocatalyst (Degussa, P-25) consisting of anatase and rutile crystalline phases. *J. Catal.* **2001**, *203*, 82–86.

[46] Li, J.; Xu, D. Tetragonal faceted-nanorods of anatase TiO_2 single crystals with a large percentage of active {100} facets. *Chem. Comm*. **2010**, *46*, 2301–2303.

[47] Zhang, D.; Li, G.; Yang, X; Yu, J. C. A micrometer-size TiO_2 single crystal photocatalyst with remarkable 80% level of reactive facets. *Chem. Comm*. **2009**, *29*, 4381–4383.